Journal of
Mechanics of Materials and Structures

ELASTIC FLEXURAL-TORSIONAL BUCKLING OF CIRCULAR ARCHES UNDER UNIFORM COMPRESSION AND EFFECTS OF LOAD HEIGHT

Mark Andrew Bradford and Yong-Lin Pi

Volume 1, Nº 7 *September 2006*

mathematical sciences publishers

JOURNAL OF MECHANICS OF MATERIALS AND STRUCTURES
Vol. 1, No. 7, 2006
dx.doi.org/10.2140/jomms.2006.1.1235

ELASTIC FLEXURAL-TORSIONAL BUCKLING OF CIRCULAR ARCHES UNDER UNIFORM COMPRESSION AND EFFECTS OF LOAD HEIGHT

MARK ANDREW BRADFORD AND YONG-LIN PI

A circular arch with in-plane radial loads uniformly distributed around the arch axis is primarily subjected to uniform compression. Under this action, the arch may suddenly deflect laterally and twist out of the plane of loading and fail in a flexural-torsional buckling mode. In most studies of the elastic flexural-torsional buckling of arches under uniform compression, the directions of the uniformly distributed loads are assumed to be unchanged and parallel to their initial directions during buckling. In practice, arches may be subjected to hydrostatic or to uniformly distributed directed radial loads. Hydrostatic loads always remain normal to the tangent of the deformed arch axis, while uniformly distributed directed radial loads always remain directed toward a specific point during buckling. These uniform radial loads may act at a load height, such as at the top surface of the cross-section. In this case, the radial loads produce an additional torsional moment during buckling which affects the flexural-torsional buckling of the arch. This paper uses both virtual work and static equilibrium approaches to study the elastic flexural-torsional buckling, effects of the load height on the buckling of circular arches under uniform compression (that is, produced by uniformly distributed dead or by directed radial loads), and closed form solutions for the buckling loads are developed.

1. Introduction

An arch with in-plane radial loads q at a load height y_q, uniformly distributed around the axis of a circular arch, is primarily subjected to a uniform compression force $Q = q(R - y_q)$, as shown in Figure 1a, where R is the radius of the initial curvature of the arch and Θ is the included angle of the arch. Under this action, the arch may suddenly deflect laterally and twist out of its plane of loading and fail in a flexural-torsional buckling mode (Figure 1b). The elastic flexural-torsional buckling of arches under uniform compression has been studied by a number of researchers. The static equilibrium approach was used by Vlasov [1961], while an energy approach was used by other researchers [Timoshenko and Gere 1961; Yoo 1982; Papangelis and Trahair 1987; Yang and Kuo 1987; Rajasekaran and Padmanabhan 1989; Kang and Yoo 1994; Bradford and Pi 2002]. With the exception of [Vlasov 1961], these studies conventionally assumed that the directions of the uniformly distributed radial loads do not change and remain parallel to their initial directions during buckling (Figure 1b (i)); this load case is called *radial dead loads* in this study for convenience. In addition to the radial dead loads, the uniform compression in a circular arch may also be assumed to be produced by hydrostatic or uniformly distributed directed radial loads, for example in the case of submerged arches. In the case of hydrostatic loads (Figure 1b (ii)), the loads always remain

This work has been supported by a Federation Fellowship, an Australian Professorial Fellowship, and a Discovery Project awarded to the first author by the Australian Research Council.

Keywords: buckling, circular arch, directed radial loads, flexural-torsional, hydrostatic loads, effect of load height, uniform compression.

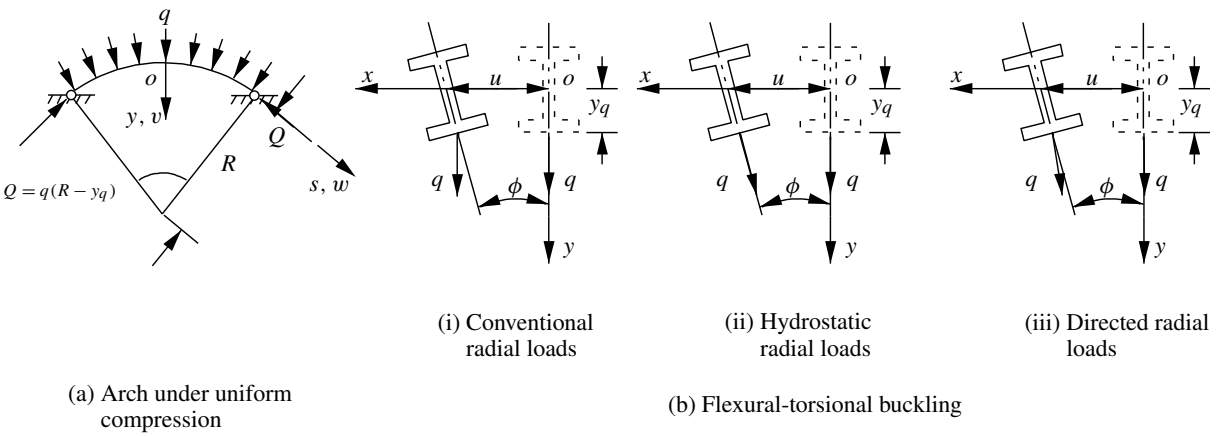

Figure 1. Flexural-torsional buckling of arches under uniform compression.

normal to the tangent of the deformed arch axis during buckling. As proved by Bolotin [1963], when both normal and tangential displacements at the boundaries vanish, hydrostatic loads are conservative because they have potentials. Hence, hydrostatic loads acting on pin-ended or fixed arches, whose radial and axial displacements vanish, are conservative. Timoshenko and Gere [1961] analyzed the in-plane buckling of circular ring and arches under the hydrostatic loads, while Vlasov [1961] studied the flexural-torsional buckling of circular arches under the hydrostatic loads. It is worth pointing out that Vlasov's result has been referenced by a number of researchers as being the result for uniformly distributed radial dead loads [Yoo 1982; Papangelis and Trahair 1987; Yang and Kuo 1987; Rajasekaran and Padmanabhan 1989; Kang and Yoo 1994; Bradford and Pi 2002]. In the case of uniformly distributed directed radial loads (Figure 1b (iii)), the loads are always directed to a specific point, such as the center of the initial curvature of the arch during buckling. A load directed to a certain point during deformation has also been proved to be conservative [Timoshenko and Gere 1961; Simitses 1976; Ings and Trahair 1987] because it also has a potential. Ings and Trahair [1987] investigated the stability of beams and columns under directed loading. Simitses [1976] and Simitses and Hodges [2006] studied the in-plane buckling of arches that are subjected to uniformly distributed radial dead loads, uniformly distributed loads always directed to the arch curvature center, and to hydrostatic loads. Simitses and Hodges [2006] also studied the flexural-torsional buckling for end-loaded cases. Timoshenko and Gere [1961] investigated the flexural-torsional buckling of arches with a narrow rectangular cross-section under the radial loads directed to the center of the initial curvature of the arch. In the buckled configuration, hydrostatic loads and uniformly distributed loads that are directed to the initial arch curvature center have lateral components in the opposite direction to that of the lateral buckling displacements. These lateral components increase the resistance of the arch to flexural-torsional buckling, and thus their effects on the flexural-torsional buckling of the arch have to be considered in the buckling analysis. The uniform radial loads that produce uniform axial compression in an arch do not necessarily act at the centroid, and they may act at a load height such as at the top surface of the cross-section. In this case, the radial loads produce an additional torsional moment during buckling which affects the flexural-torsional buckling behavior of the arch, and so the effects of the load height on the flexural-torsional buckling of arches under uniform compression warrant investigation.

Trahair and Papangelis [1987] and Trahair [1993] investigated effects of the load height on the flexural-torsional buckling of arches under uniform compression produced by uniformly distributed radial dead loads. However, comprehensive studies of the elastic flexural-torsional buckling of arches under uniform compression produced by dead or directed uniformly distributed radial loads or by hydrostatic loads, and of the effects of the load height on the flexural-torsional buckling, do not appear to have been reported.

The purpose of this paper is to use both virtual work and static equilibrium approaches to study the elastic flexural-torsional buckling and the effects of the load height on the buckling of circular arches under uniform compression produced by dead, or directed uniformly distributed radial loads, or by hydrostatic loads, and to derive the buckling loads in closed form. The principle of virtual work will lead to the equilibrium equations in weak form, while the static equilibrium approach will lead to the differential equilibrium equations directly.

2. Curvatures and strains

2.1. ***Rotations and curvatures.*** The basic assumptions used in this investigation are:

(1) Euler–Bernoulli bending theory and Vlasov's torsion theory are used, so the cross-sections are assumed to remain rigid in their plane (that is, not to distort during deformation), and local buckling and/or effects of distortion of the cross-section are excluded;

(2) the arches are circular and of doubly symmetric uniform cross-section, so the centroid of the cross-section coincides with its shear center;

(3) the height D of the cross-section is much smaller than both the length S and the radius R of the initial curvature of the arch, that is, $D/S \ll 1$ and $D/R \ll 1$.

A body-attached curvilinear orthogonal axis system $oxys$ is defined as follows. The axis os passes through the locus of the centroids of the cross-section of the undeformed arch, and the axes ox and oy coincide with the principal axes of the cross-section, as shown in Figures 1 and 2. In the undeformed configuration, the axis oy is toward the center of the arch. After the deformation, the origin o displaces laterally u, radially v, and axially w to o_1 and the cross-section rotates through an angle ϕ, and so the body-attached curvilinear orthogonal axis system $oxys$ moves and rotates to a new position $o_1x_1y_1s_1$, as shown in Figures 2 and 3. In the axis system $oxys$, the initial curvature κ_{x0} of the centroidal axis os of a circular arch about the major principal axis ox is defined as positive (that is, in the direction of the minor principal axis oy of the cross-section), and so $\kappa_{x0} = -1/R$ for arches with the upward rise as shown in Figure 1. This definition for the initial curvature is consistent with the definition of the curvature after deformation.

A unit vector $\mathbf{p}_s$ in the tangent direction of the axis os, and unit vectors $\mathbf{p}_x$ and $\mathbf{p}_y$ in the direction of the axes ox and oy (Figures 2 and 3) are used as the fixed reference basis. They do not change with the deformation, but their directions change from point to point along the arch axis os. In the deformed configuration, a unit vector $\mathbf{q}_s$ is defined in the tangent direction of the axis o_1s_1 of the axis system $o_1x_1y_1s_1$, and unit vectors $\mathbf{q}_x$ and $\mathbf{q}_y$ are defined in the principal axes o_1x_1, o_1y_1 of the rotated cross-section at o_1, as shown in Figure 2. The unit vectors $\mathbf{q}_x$, $\mathbf{q}_y$, $\mathbf{q}_s$ are attached to the arch and move with it during the deformation with the vector $\mathbf{q}_s$, being normal to the cross-section at all times.

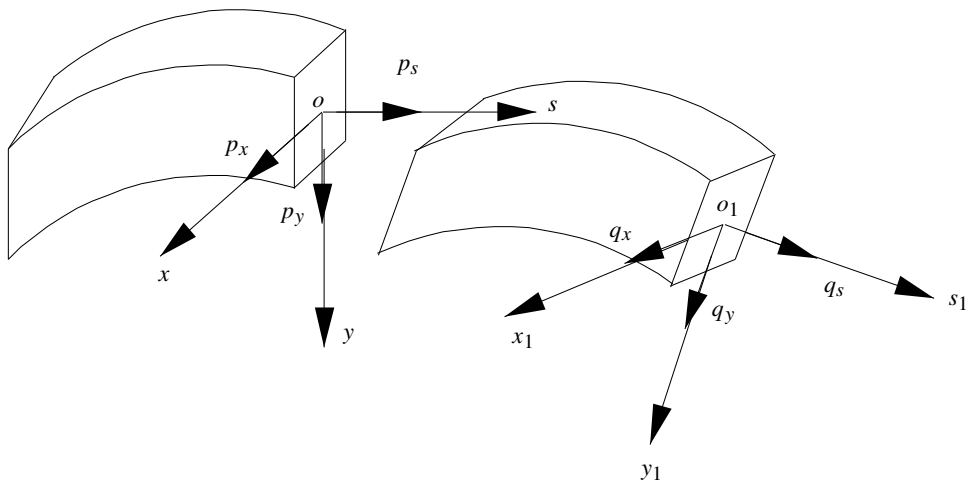

Figure 2. Kinematics during buckling.

The rotation from the basis vectors $\mathbf{p}_x$, $\mathbf{p}_y$, $\mathbf{p}_s$ in the undeformed configuration to the basis vectors $\mathbf{q}_x$, $\mathbf{q}_y$, $\mathbf{q}_s$ in the deformed configuration (Figures 2 and 3) can be expressed [Pi and Bradford 2004] using a rotation matrix $\mathbf{R}$ as

$$\begin{bmatrix} \mathbf{q_x} \\ \mathbf{q_y} \\ \mathbf{q_s} \end{bmatrix} = \begin{bmatrix} R_{xx} & R_{xy} & R_{xs} \\ R_{yx} & R_{yy} & R_{ys} \\ R_{sx} & R_{sy} & R_{ss} \end{bmatrix} \begin{bmatrix} \mathbf{p_x} \\ \mathbf{p_y} \\ \mathbf{p_s} \end{bmatrix}, \tag{1}$$

where

$$\begin{aligned} R_{xx} &= (1-\lambda\hat{u}'^2)C - \lambda\hat{u}'\hat{v}'S, & R_{xy} &= -(1-\lambda\hat{u}'^2)S - \lambda\hat{u}'\hat{v}'C, & R_{xs} &= \hat{u}', \\ R_{yx} &= (1-\lambda\hat{v}'^2)S - \lambda\hat{u}'\hat{v}'C, & R_{yy} &= (1-\lambda\hat{v}'^2)C + \lambda\hat{u}'\hat{v}'S, & R_{ys} &= \hat{v}', \\ R_{sx} &= -\hat{u}'C - \hat{v}'S, & R_{sy} &= \hat{u}'S - \hat{v}'C, & R_{ss} &= \hat{w}', \end{aligned}$$

in which $C \equiv \cos\phi$, $S \equiv \sin\phi$, $\hat{u}' = u'/(1+\epsilon)$, $\hat{v}' = \tilde{v}'/(1+\epsilon)$, $\hat{w}' = (1+\tilde{w}')/(1+\epsilon)$, $\tilde{v}' = v' - w\kappa_{x0}$, $\tilde{w}' = w' + v\kappa_{x0}$, $(\,)' \equiv \mathrm{d}(\,)/\mathrm{d}s$, $(1+\epsilon) = \sqrt{(u')^2 + (\tilde{v}')^2 + (1+\tilde{w}')^2}$, $\lambda = 1/(1+\hat{w}')$.

The rotation matrix $\mathbf{R}$ in Equation (1) belongs to a special orthogonal rotation group denoted $SO(3)$ because it satisfies the orthogonality and unimodular conditions that $\mathbf{R}\mathbf{R}^T = \mathbf{R}^T\mathbf{R} = \mathbf{I}$ and $\det \mathbf{R} = +1$ [Burn 1985].

It can be shown [Pi and Bradford 2004] that the material curvatures in the deformed configuration can be obtained from the rotation matrix $\mathbf{R}$ as

$$(1+\epsilon)\mathbf{K} = \mathbf{R}^T \frac{\mathrm{d}\mathbf{R}}{\mathrm{d}s} + \mathbf{R}^T\mathbf{K}_0\mathbf{R}, \tag{2}$$

where

$$\mathbf{K}_0 = \begin{bmatrix} 0 & 0 & 0 \\ 0 & 0 & -\kappa_{x0} \\ 0 & \kappa_{x0} & 0 \end{bmatrix} = \frac{1}{R}\begin{bmatrix} 0 & 0 & 0 \\ 0 & 0 & 1 \\ 0 & -1 & 0 \end{bmatrix} \quad \text{and} \quad \mathbf{K} = \begin{bmatrix} 0 & -\kappa_s & \kappa_y \\ \kappa_s & 0 & -\kappa_x \\ -\kappa_y & \kappa_x & 0 \end{bmatrix}, \tag{3}$$

in which κ_x and κ_y are the material curvatures about the unit vectors $\mathbf{q}_x$ and $\mathbf{q}_y$, that is, about the positive direction of the axes o_1x_1 and o_1y_1, and κ_s is the material twist per unit length about the unit vector $\mathbf{q}_s$, that is, about the positive direction of the o_1s_1 axis in the deformed configuration.

Substituting Equation (1) and the first equation of Equation (3) into Equation (2) leads to the curvatures κ_x and κ_y and the twist κ_s, expressed explicitly as

$$\begin{aligned}
\kappa_x &= \{\hat{u}''S - \hat{v}''C - \lambda\hat{w}''(\hat{u}'S - \hat{v}'C) + [\lambda(1 - \hat{u}'^2 - \hat{w}'^2)C - \lambda\hat{u}'\hat{v}'S + \hat{w}'C]\kappa_{x0}\}(1+\epsilon)^{-1}, \\
\kappa_y &= \{\hat{u}''C + \hat{v}''S - \lambda\hat{w}''(\hat{u}'C + \hat{v}'S) - [\lambda(1 - \hat{u}'^2 - \hat{w}'^2)S + \lambda\hat{u}'\hat{v}'C + \hat{w}'S]\kappa_{x0}\}(1+\epsilon)^{-1}, \\
\kappa_s &= [\phi' + \lambda(\hat{u}''\hat{v}' - \hat{u}'\hat{v}'') + \hat{u}'\kappa_{x0}](1+\epsilon)^{-1}.
\end{aligned}$$

2.2. ***Strains and displacements of load points.*** The position vector $\mathbf{a}_0$ of an arbitrary point $P(x, y)$ on the cross-section in the undeformed configuration can be expressed as $\mathbf{a}_0 = \mathbf{r}_0 + x\mathbf{p}_x + y\mathbf{p}_y$ (see Figure 3), where $\mathbf{r}_0$ is the position vector of the centroid o, related to the unit vector $\mathbf{p}_s$ by $\mathbf{p}_s = \mathrm{d}\mathbf{r}_0/\mathrm{d}s$, and the

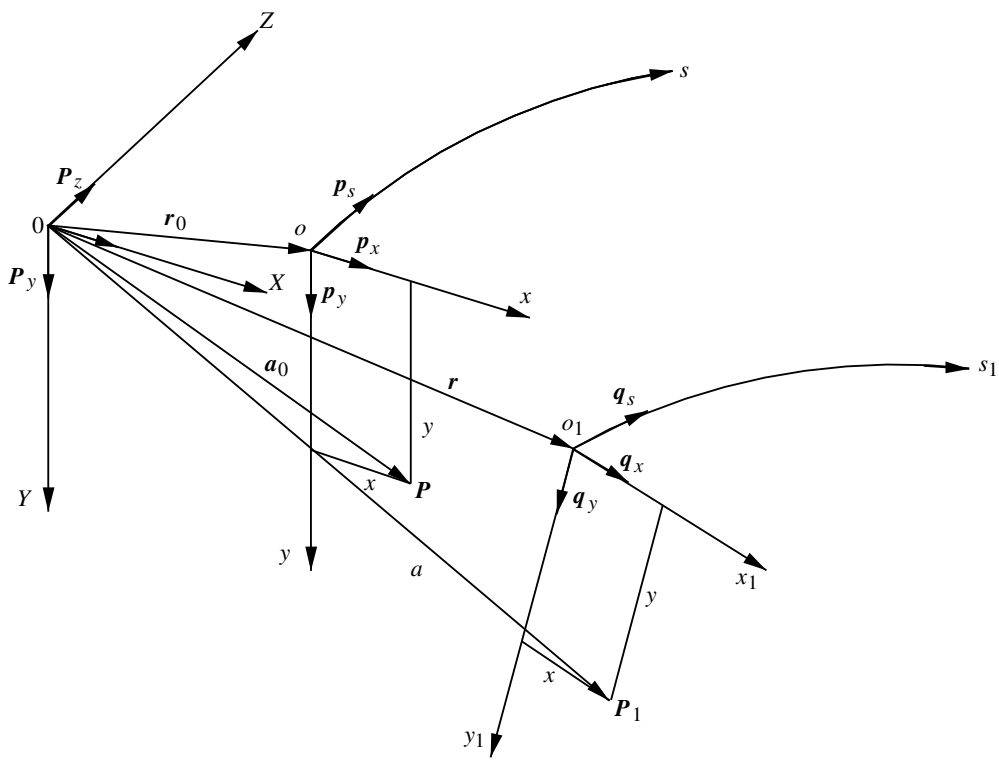

Figure 3. Position vectors.

initial gradient tensor $\mathbf{F}_0$ in the undeformed configuration can be expressed as

$$\mathbf{F}_0 = \left(\frac{\partial \mathbf{a}_0}{\partial x}, \frac{\partial \mathbf{a}_0}{\partial y}, \frac{\partial \mathbf{a}_0}{\partial s}\right). \tag{4}$$

The position of the point $P(\mathrm{x}, \mathrm{y})$ in the deformed configuration is determined based on the assumption that the total displacement of a point P results from two successive motions: translation and rotation of the cross-section, and a superimposed warping displacement along the unit vector $\mathbf{q}_s$ in the deformed configuration. The position vector $\mathbf{a}$ of the point P in the deformed configuration can be expressed as $\mathbf{a} = \mathbf{r} + x\mathbf{q}_x + y\mathbf{q}_y - \omega(x, y)\kappa_s\mathbf{q}_s$ (see Figure 3), in which $\omega(x, y)$ is the warping function and $\mathbf{r}$ is the position vector of the centroid o_1 in the deformed configuration and is given by $\mathbf{r} = \mathbf{r}_0 + u\mathbf{p}_x + v\mathbf{p}_y + w\mathbf{p}_s$.

The deformation gradient tensor $\mathbf{F}$ can then be expressed as

$$\mathbf{F} = \left(\frac{\partial \mathbf{a}}{\partial x}, \frac{\partial \mathbf{a}}{\partial y}, \frac{\partial \mathbf{a}}{\partial s}\right) = \left(\frac{\partial \mathbf{a}}{\partial x}, \frac{\partial \mathbf{a}}{\partial y}, (1+\epsilon)\frac{\partial \mathbf{a}}{\partial s_1}\right), \tag{5}$$

and so the strain tensor can be expressed in terms of the initial and deformation gradient tensors as

$$\begin{bmatrix} \epsilon_{xx} & \frac{1}{2}\gamma_{xy} & \frac{1}{2}\gamma_{xs} \\ \frac{1}{2}\gamma_{yx} & \epsilon_{yy} & \frac{1}{2}\gamma_{ys} \\ \frac{1}{2}\gamma_{sx} & \frac{1}{2}\gamma_{sy} & \epsilon_{ss} \end{bmatrix} = \frac{1}{2}\left(\mathbf{F}^T\mathbf{F} - \mathbf{F}_0^T\mathbf{F}_0\right). \tag{6}$$

Substituting Equations (4) and (5) into Equation (6) yields

$$\epsilon_{xx} = \epsilon_{yy} = \gamma_{xy} = 0, \tag{7}$$

$$\begin{aligned} \epsilon_{ss} = {} & \tilde{w}' + \tfrac{1}{2}u'^2 + \tfrac{1}{2}\tilde{v}'^2 - x\kappa_y + y\kappa_x - \omega\kappa_s' + \tfrac{1}{2}\left(x^2+y^2\right)\kappa_s^2 = \tilde{w}' + \tfrac{1}{2}u'^2 + \tfrac{1}{2}\tilde{v}'^2 \\ & - x(u''\cos\phi + \tilde{v}''\sin\phi - \kappa_{x0}\sin\phi) + y\left(u''\sin\phi - \tilde{v}''\cos\phi + \left(\cos\phi - 1 - \tfrac{1}{2}u'^2\right)\kappa_{x0}\right) \\ & - \omega(\phi'' + u''\kappa_{x0}) + \tfrac{1}{2}\left(x^2+y^2\right)(\phi' + u'\kappa_{x0})^2, \end{aligned} \tag{8}$$

$$\gamma_{sx} = -\left(y + \frac{\partial\omega}{\partial x}\right)\kappa_s = -\left(y + \frac{\partial\omega}{\partial x}\right)(\phi' + u'\kappa_{x0}), \tag{9}$$

$$\gamma_{sy} = \left(x - \frac{\partial\omega}{\partial y}\right)\kappa_s = \left(x - \frac{\partial\omega}{\partial y}\right)(\phi' + u'\kappa_{x0}), \tag{10}$$

where ϵ_{ss} is the longitudinal normal strain and γ_{sx} and γ_{sy} are the uniform torsional shear strains at an arbitrary point $P(x,\ y)$ on the cross-section.

It is assumed that the uniform radial loads q are acting at a load position $(0,\ y_q)$, where y_q is the radial coordinate of the point of application load q. The displacements of the load point at the position $(0,\ y_q)$ are given by

$$\begin{bmatrix} u_q \\ v_q \\ w_q \end{bmatrix} = \begin{bmatrix} u \\ v \\ w \end{bmatrix} + \mathbf{R}\begin{bmatrix} 0 \\ y_q \\ 0 \end{bmatrix} - \begin{bmatrix} 0 \\ -y_q \\ 0 \end{bmatrix} \approx \begin{bmatrix} u - y_q\left(\phi - \frac{1}{2}u'\tilde{v}'\right) \\ v - \frac{1}{2}y_q\left(\phi^2 - \tilde{v}'^2\right) \\ \tilde{w} + y_q\tilde{v}' \end{bmatrix}, \tag{11}$$

where the third and higher-order terms have been ignored.

3. Virtual work approach

3.1. ***Virtual work and equilibrium equations.*** Because all three load cases are conservative, the problem can be treated using energy methods such as the minimum potential energy method or virtual work method [Simitses 1976; Guran 2000; Simitses and Hodges 2006]. The principle of virtual work is used in this paper. When the uniform radial load q acts at a load height y_q, the principle of virtual work for the equilibrium of the arch in the buckled configuration can then be stated as

$$\delta\Pi = \int_V (E\epsilon_{ss}\delta\epsilon_{ss} + G\gamma_{sx}\delta\gamma_{sx} + G\gamma_{sy}\delta\gamma_{sy})\,\mathrm{d}V - \int_0^S (q_{ex}\delta u_q + q_{ey}\delta v_q)\frac{R - y_q}{R}\,\mathrm{d}s = 0, \tag{12}$$

for all kinematically admissible sets of infinitesimal virtual displacements $\{\delta u, \delta v, \delta w, \delta\phi\}$, where the compatible strains ϵ_{ss}, γ_{sx} and γ_{sy} are given by Equations (8)–(10) and the compatible displacements u_q and v_q of the load point are given by Equation (11), and where V indicates the volume of the arch, E and G are the Young's and shear moduli of elasticity, q_{ex} and q_{ey} are the lateral and radial components of the uniform load q, as shown in Figure 4, and $\delta(\,)$ denotes the Lagrange operator of simultaneous variations.

During flexural-torsional buckling, the in-plane deformations are constant and thus the variations of the in-plane deformations vanish, so that $\delta v = \delta v' = \delta v'' = \delta w = \delta w' = \delta w'' = 0$. By substituting Equations (7)–(11) into Equation (12), and considering that the initial curvature $\kappa_{x0} = -1/R$, that the bending moment $M = 0$ under uniform compression, and that the axial stress resultant $N = \int_A E\epsilon_{ss}\mathrm{d}A = -Q = -q(R - y_q)$, the statement for the principle of virtual work given by Equation (12) can be expressed

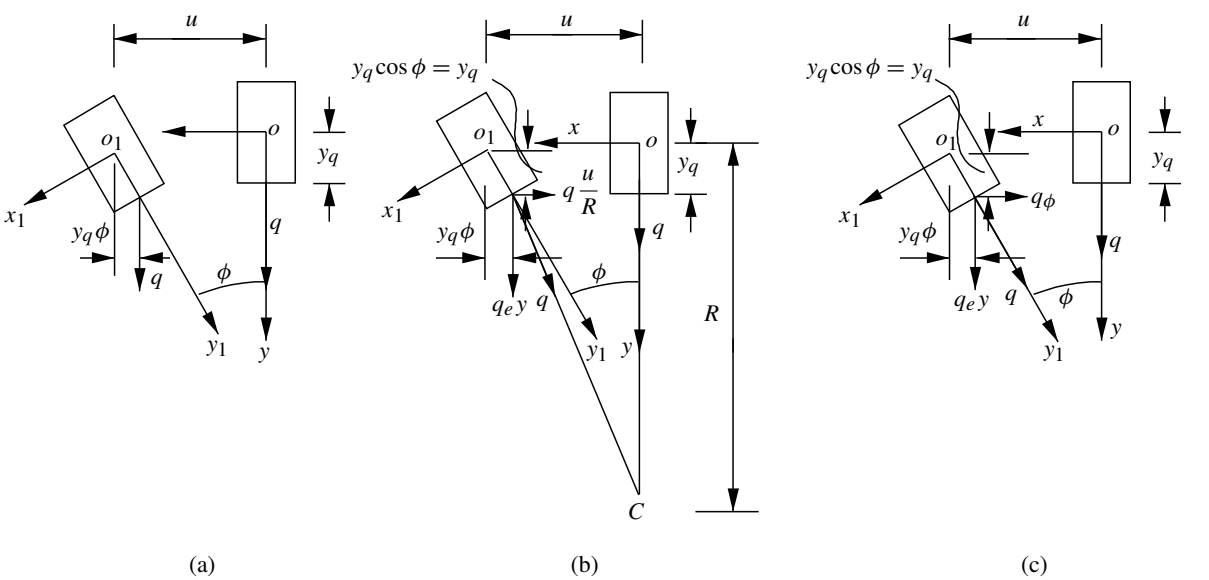

Figure 4. Lateral and radial components of uniform loads. (a) Radial dead loads (load case I); (b) radial loads directed toward arch center (load case II); (c) hydrostatic radial loads (load case III).

as

$$\delta\Pi = \int_0^S \left(EI_y\left(u'' + \frac{\phi}{R}\right)\left(\delta u'' + \frac{\delta\phi}{R}\right) + GJ\left(\phi' - \frac{u'}{R}\right)\left(\delta\phi' - \frac{\delta u'}{R}\right) + EI_w\left(\phi'' - \frac{u''}{R}\right)\left(\delta\phi'' - \frac{\delta u''}{R}\right) \right.$$
$$\left. - Q\left(u'\delta u' + r_0^2\left(\phi' - \frac{u'}{R}\right)\left(\delta\phi' - \frac{\delta u'}{R}\right)\right) + \left(q_{ey}y_q\phi\delta\phi - q_{ex}(\delta u - y_q\delta\phi)\right)\frac{R - y_q}{R}\right) \mathrm{d}s = 0, \quad (13)$$

where I_y is the second moment of area of the cross-section about its minor principal axis, J is the Saint-Venant torsion constant, I_w is the warping constant of the cross-section, and the term

$$\left(-Qr_0^2(\phi' - u'/R)(\delta\phi' - \delta u'/R)\right),$$

represents the virtual work due to Wagner effects [Hodges 2006] with the cross-sectional radius of gyration r_0 being defined by $r_0 = \sqrt{(I_x + I_y)/A}$.

Integrating Equation (13) by parts leads to the differential equilibrium equations for the flexural-torsional buckling

$$\left(EI_y\left(u'' + \frac{\phi}{R}\right)\right)'' + \left(GJ\left(\phi' - \frac{u'}{R}\right)\frac{1}{R}\right)' - \left(EI_w\left(\phi'' - \frac{u''}{R}\right)\frac{1}{R}\right)''$$
$$+ \left(Q\left(u' - r_0^2\left(\phi' - \frac{u'}{R}\right)\frac{1}{R}\right)\right)' - q_{ex}\frac{R - y_q}{R} = 0, \quad (14)$$

$$EI_y\left(u'' + \frac{\phi}{R}\right)\frac{1}{R} - \left(GJ\left(\phi' - \frac{u'}{R}\right)\right)' + \left(EI_w\left(\phi'' - \frac{u''}{R}\right)\right)'' + \left(r_0^2 Q\left(\phi' - \frac{u'}{R}\right)\right)'$$
$$+ \left(q_{ey}y_q\phi + q_{ex}y_q\right)\frac{R - y_q}{R} = 0, \quad (15)$$

and to the static boundary conditions at both ends of the arch ($s = 0$ and $s = S$)

$$\left(\left(EI_y\left(u'' + \frac{\phi}{R}\right)\right)' + \left(GJ\left(\phi' - \frac{u'}{R}\right)\frac{1}{R}\right) - \left(EI_w\left(\phi'' - \frac{u''}{R}\right)\frac{1}{R}\right)' + Qu' - Q\left(\phi' - \frac{u'}{R}\right)\frac{r_0^2}{R}\right)\delta u = 0, \quad (16)$$

$$\left(\left(EI_y\left(u'' + \frac{\phi}{R}\right)\right) - \left(EI_w\left(\phi'' - \frac{u''}{R}\right)\frac{1}{R}\right)\right)\delta u' = 0, \quad (17)$$

$$\left(GJ\left(\phi' - \frac{u'}{R}\right) - \left(EI_w\left(\phi'' - \frac{u''}{R}\right)\right)' - Qr_0^2\left(\phi' - \frac{u'}{R}\right)\right)\delta\phi = 0, \quad (18)$$

$$EI_w\left(\phi'' - \frac{u''}{R}\right)\delta\phi' = 0. \quad (19)$$

In addition, the kinematic boundary conditions for pin-ended arches, such that

$$u = \phi = 0 \qquad \text{at} \quad s = 0 \quad \text{and} \quad s = S, \quad (20)$$

also need to be satisfied. For a laterally pin-ended arch, the buckling deformations $u'' = \phi'' = 0$ at its boundaries and the variations $\delta u = \delta\phi = 0$, so that the static boundary conditions given by Equations (16)–(19) are satisfied.

Three cases of the uniformly distributed loads q are considered. In the case of radial dead loads (load case I), it is assumed that the directions of the loads do not change during buckling and that the loads remain parallel to their initial directions, as shown in Figure 4a. In this case, the loads q have lateral and radial components, q_{ey} and q_{ex}, given by

$$q_{ex} = 0, \qquad q_{ey} = q = \frac{Q}{R - y_q}. \tag{21}$$

This case has been studied by a number of researchers [Timoshenko and Gere 1961; Yoo 1982; Papangelis and Trahair 1987; Yang and Kuo 1987; Rajasekaran and Padmanabhan 1989; Kang and Yoo 1994; Bradford and Pi 2002].

In the case of directed radial loads (load case II), the loads q are assumed to be always directed toward the center of the initial curvature of the arch as shown in Figure 4b during buckling. In this case, the loads q have lateral and radial components, q_{ey} and q_{ex}, given by

$$q_{ex} \approx -\frac{qu}{R} = -\frac{Qu}{R(R - y_q)}, \qquad q_{ey} \approx q = \frac{Q}{R - y_q}. \tag{22}$$

In the case of hydrostatic loads (load case III), the loads q are assumed to be mechanically hydrostatic, that is, the loads q change their directions slightly but always remain normal to the tangent of the deformed arch axis (that is, remain in the direction of the axis $o_1 y_1$ of the cross-section) during buckling, as shown in Figure 4c. In this case, the hydrostatic loads q have the lateral and radial components, q_{ex} and q_{ey}, given by

$$q_{ex} = -q \sin\phi \approx -q\phi = -\frac{Q\phi}{R - y_q}, \qquad q_{ey} = q\cos\phi \approx q = \frac{Q}{R - y_q}, \tag{23}$$

where $\sin\phi \approx \phi$ and $\cos\phi \approx 1$, since the buckling displacements ϕ are infinitesimally small.

It can be seen from Figure 4 and from Equations (22) and (23) that during buckling, the lateral components q_{ex} of directed radial loads and of hydrostatic loads acting on an arch are in opposite directions to the lateral buckling displacements. The lateral components q_{ex} are expected to produce combined torsion and lateral bending actions that oppose the flexural-torsional buckling, so the flexural-torsional buckling loads of the arch will increase.

3.2. ***Solutions for flexural-torsional buckling loads.*** The n-th mode buckled shapes of a laterally pin-ended arch can be assumed to be given by

$$\frac{u}{u_m} = \frac{\phi}{\phi_m} = \sin\frac{n\pi s}{S}, \tag{24}$$

which satisfies the kinematic boundary conditions given by Equation (20), and where u_m and ϕ_m are the maximum lateral displacement of the centroid and the twist angle of the cross-section during buckling, and n is the number of buckled half waves. Substituting Equations (21), (22) or (23), and Equation (24)

into Equations (14) and (15) leads to

$$\begin{bmatrix} k_{11} & k_{12} \\ k_{21} & k_{22} \end{bmatrix} \begin{bmatrix} u_m \\ \phi_m \end{bmatrix} = \begin{bmatrix} 0 \\ 0 \end{bmatrix}, \tag{25}$$

where the coefficients k_{11}, k_{12}, k_{21}, and k_{22} are given by

$$k_{11} = \begin{cases} \left(1 + a_n^2 b_n^2 - \left(1 + a_n^2 b_n^2 \frac{P_{yn}}{P_{sn}}\right) \frac{Q}{P_{yn}}\right) P_{yn}, & \text{for load case I,} \\ \left(1 + a_n^2 b_n^2 - \left(1 - a_n^2 + a_n^2 b_n^2 \frac{P_{yn}}{P_{sn}}\right) \frac{Q}{P_{yn}}\right) P_{yn}, & \text{for load case II,} \\ \left(1 + a_n^2 b_n^2 - \left(1 + a_n^2 b_n^2 \frac{P_{yn}}{P_{sn}}\right) \frac{Q}{P_{yn}}\right) P_{yn}, & \text{for load case III,} \end{cases} \tag{26}$$

$$k_{12} = \begin{cases} -\left(\frac{a_n}{b_n} + a_n b_n - a_n b_n \frac{P_{yn}}{P_{sn}} \frac{Q}{P_{yn}}\right) M_{ysn}, & \text{for load case I,} \\ -\left(\frac{a_n}{b_n} + a_n b_n - a_n b_n \frac{P_{yn}}{P_{sn}} \frac{Q}{P_{yn}}\right) M_{ysn}, & \text{for load case II,} \\ -\left(\frac{a_n}{b_n} + a_n b_n - \left(\frac{a_n}{b_n} + a_n b_n \frac{P_{yn}}{P_{sn}}\right) \frac{Q}{P_{yn}}\right) M_{ysn}, & \text{for load case III,} \end{cases} \tag{27}$$

$$k_{21} = \begin{cases} -\left(\frac{a_n}{b_n} + a_n b_n - a_n b_n \frac{P_{yn}}{P_{sn}} \frac{Q}{P_{yn}}\right) M_{ysn}, & \text{for load case I,} \\ -\left(\frac{a_n}{b_n} + a_n b_n - \left(a_n b_n \frac{P_{yn}}{P_{sn}} - \frac{a_n}{b_n} \frac{y_q}{R}\right) \frac{Q}{P_{yn}}\right) M_{ysn}, & \text{for load case II,} \\ -\left(\frac{a_n}{b_n} + a_n b_n - a_n b_n \frac{P_{yn}}{P_{sn}} \frac{Q}{P_{yn}}\right) M_{ysn}, & \text{for load case III,} \end{cases} \tag{28}$$

$$k_{22} = \begin{cases} \left(1 + \frac{a_n^2}{b_n^2} - \left(\frac{P_{yn}}{P_{sn}} - \frac{y_q}{R b_n^2}\right) \frac{Q}{P_{yn}}\right) r_0^2 P_{sn}, & \text{for load case I,} \\ \left(1 + \frac{a_n^2}{b_n^2} - \left(\frac{P_{yn}}{P_{sn}} - \frac{y_q}{R b_n^2}\right) \frac{Q}{P_{yn}}\right) r_0^2 P_{sn}, & \text{for load case II,} \\ \left(1 + \frac{a_n^2}{b_n^2} - \frac{P_{yn}}{P_{sn}} \frac{Q}{P_{yn}}\right) r_0^2 P_{sn}, & \text{for load case III.} \end{cases} \tag{29}$$

In Equations (26)–(29), P_{yn} is the n-th mode elastic flexural buckling load of a pin-ended column of length S under uniform compression about the minor principal axis of its cross-section, P_{sn} is the n-th mode elastic torsional buckling load of a pin-ended column of length S under uniform compression, and M_{ysn} is the n-th mode elastic flexural-torsional buckling moment of a simply supported beam of length S under uniform bending. It is well known that P_{yn}, P_{sn} and M_{ysn} are given by [Trahair 1993; Trahair and Bradford 1998]

$$P_{yn} = \frac{(n\pi)^2 E I_y}{S^2}, \qquad P_{sn} = \frac{1}{r_0^2}\left(G J + \frac{(n\pi)^2 E I_w}{S^2}\right), \qquad M_{ysn} = \sqrt{r_0^2 P_{yn} P_{sn}}, \qquad r_0^2 = \frac{I_x + I_y}{A}.$$

The parameters a_n and b_n are defined as

$$a_n = \frac{S}{n\pi R}, \qquad b_n = \frac{n\pi M_{ysn}}{P_{yn} S}.$$

Equation (25) has nontrivial solutions for u_m and ϕ_m when the determinant of its coefficient matrix vanishes, that is, when $k_{11}k_{22} - k_{12}k_{21} = 0$, which leads to the generic equation for the elastic flexural-torsional buckling load of a pin-ended arch under uniform compression produced by uniformly distributed

radial loads,

$$A_1\left(\frac{Q}{P_{yn}}\right)^2 + B_1\frac{Q}{P_{yn}} + C_1 = 0, \tag{30}$$

where the coefficients for load cases I, II, and III are, respectively,

$$\begin{aligned} A_1 &= \frac{P_{yn}}{P_{sn}} - \left(1 + a_n^2 b_n^2 \frac{P_{yn}}{P_{sn}}\right)\frac{y_q}{Rb_n^2}, \\ B_1 &= -\left(\left(1 + \frac{a_n^2}{b_n^2}\right) + \left(1 - a_n^2\right)^2 \frac{P_{yn}}{P_{sn}} - (1 + a_n^2 b_n^2)\,\frac{y_q}{Rb_n^2}\right), \\ C_1 &= (1 - a_n^2)^2; \end{aligned} \tag{31}$$

$$\begin{aligned} A_1 &= \frac{P_{yn}}{P_{sn}} - \frac{y_q}{Rb_n^2}, \\ B_1 &= -\left(1 + \frac{a_n^2}{b_n^2} + (1 - a_n^2)\,\frac{P_{yn}}{P_{sn}} - \frac{y_q}{Rb_n^2}\right), \\ C_1 &= 1 - a_n^2; \end{aligned} \tag{32}$$

$$\begin{aligned} A_1 &= 1, \\ B_1 &= -\left(\frac{P_{sn}}{P_{yn}} + (1 - a_n^2)\right), \\ C_1 &= (1 - a_n^2)\,\frac{P_{sn}}{P_{yn}}. \end{aligned} \tag{33}$$

It can be seen from Equations (31) and (32) that the load height y_q affects the flexural-torsional buckling of an arch in the cases of dead or directed uniformly distributed radial loads (load cases I and II). However, Equation (33) indicates that the load height y_q of hydrostatic loads (load case III) has no effect on the flexural-torsional buckling of an arch. When the radial loads act at the centroid ($y_q = 0$), it can be demonstrated that for the same arch, the buckling load for load case III given by Equations (30) and (33) is the highest, while the buckling load for load case I given by Equations (30) and (31) is the lowest.

4. Static equilibrium approach

A static equilibrium approach is used in this section to investigate the flexural-torsional buckling and the effects of the load height on the buckling of arches under uniform compression, and to verify the solutions obtained by the virtual work approach in the previous section. In the buckled configuration, the axial compressive force Q in the axis os has an axial compressive component $Q_{es} \approx Q$ in the axis $o_1 s_1$ (see Figure 5a) which produces a torsional moment action M_{es} given by

$$M_{es} = r_0^2 Q_{es}\kappa_s = r_0^2 Q_{es}\left(\phi' - \frac{u'}{R}\right) = r_0^2 Q\left(\phi' - \frac{u'}{R}\right).$$

The uniform torsional resistance M_{iu} about the axis o_1s_1 and the bimoment resistance B_i of the cross-section are given by

$$M_{iu} = GJ\kappa_s = GJ\left(\phi' - \frac{u'}{R}\right), \qquad B_i = -EI_w\kappa_s' = -EI_w\left(\phi'' - \frac{u''}{R}\right).$$

It is well known that the bimoment resistance B_i induces a warping torsional resistance M_{iw} as $M_{iw} = \mathrm{d}B_i/\mathrm{d}s$ [Vlasov 1961; Trahair and Bradford 1998]. The total torsional resistance M_{is} can be obtained by combining the uniform and warping torsional resistances M_{iu} and M_{iw} as

$$M_{is} = M_{iu} + M_{iw} = GJ\left(\phi' - \frac{u'}{R}\right) - EI_w\left(\phi''' - \frac{u'''}{R}\right).$$

In a straight member, the torsional action is in equilibrium with the torsional resistance. However, in an arch, the torsional action couples with the lateral bending action while the torsional resistance also couples with the lateral bending resistance. Hence, the resultant of the torsional action and resistance at a cross-section of an arch does not vanish. The resultant torsional moment at the cross-section is then

$$M_s = M_{es} - M_{is} = r_0^2 Q\left(\phi' - \frac{u'}{R}\right) - GJ\left(\phi' - \frac{u'}{R}\right) + EI_w\left(\phi''' - \frac{u'''}{R}\right), \tag{34}$$

where the first term is historically called the trapeze effect, the bifilar effect, Wagner's term, or Buckley's term; the second term is St. Venant torsion moment; and the third term is the warping torsion moment (Vlasov's term) [Hodges 2006].

In the buckled configuration, the axial compressive force Q in the axis os also has a lateral component Q_{ex} in the axis o_1x_1 given by $Q_{ex} = -Qu'$ (see Figure 5a). The resultant lateral bending moment at the cross-section is then equal to the lateral bending resistance M_{iy} of the cross-section about the axis o_1y_1

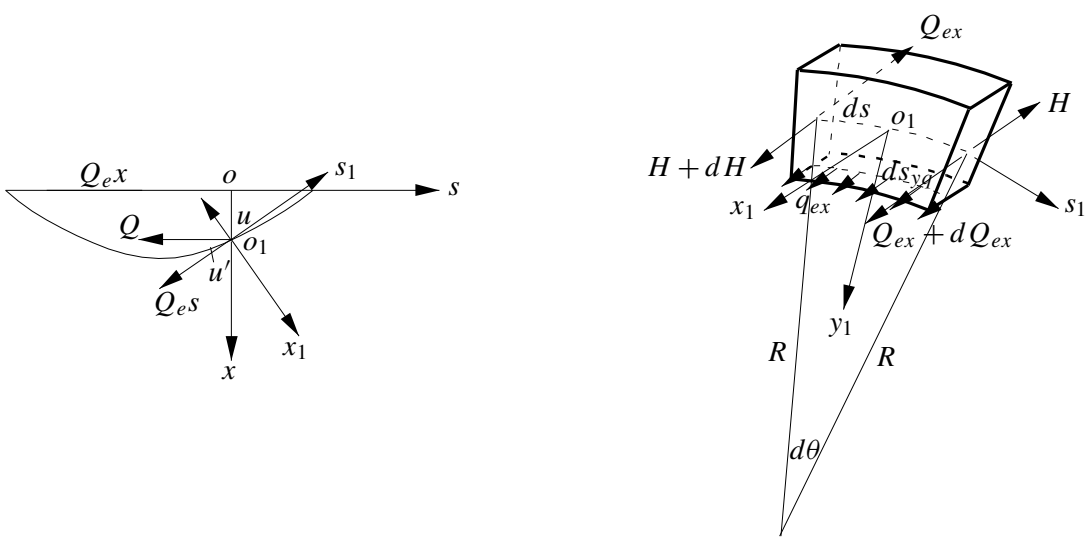

(a) components of compressive force (b) lateral force equilibrium

Figure 5. Lateral force equilibrium.

and is given by

$$M_y = M_{iy} = -EI_y\left(u'' + \frac{\phi}{R}\right). \tag{35}$$

The differential equilibrium equations in the buckled configuration can be established by considering the lateral and torsional equilibrium of a free body of a differential element ds of the arch, as shown in Figures 5 and 6. For lateral force equilibrium, it can be shown from Figure 5b that

$$H + \mathrm{d}H - H + Q_{ex} + \mathrm{d}Q_{ex} - Q_{ex} + q_{ex}\mathrm{d}s_{sq} = 0, \tag{36}$$

where $\mathrm{d}s_{sq} = [(R - y_q)/R]\,\mathrm{d}s$ and H is the internal lateral shear force. From Equation (36),

$$\frac{\mathrm{d}H}{\mathrm{d}s} = -\frac{\mathrm{d}Q_{ex}}{\mathrm{d}s} - q_{ex}\frac{R - y_q}{R}. \tag{37}$$

For lateral moment equilibrium, it can be shown from Figure 6 that

$$(M_y + \mathrm{d}M_y) - M_y + 2M_s \sin\frac{\mathrm{d}\theta}{2} + Q_x\mathrm{d}s = \mathrm{d}M_y + \frac{M_s}{R}\,\mathrm{d}s - H\mathrm{d}s = 0, \tag{38}$$

from which

$$H = \frac{\mathrm{d}M_y}{\mathrm{d}s} + \frac{M_s}{R}. \tag{39}$$

Substituting Equation (39) into Equation (37) yields the differential equilibrium equation for the lateral buckling deformation

$$\frac{\mathrm{d}^2M_y}{\mathrm{d}s^2} + \frac{\mathrm{d}M_s}{\mathrm{d}s}\frac{1}{R} + \frac{\mathrm{d}Q_{ex}}{\mathrm{d}s} + q_{ex}\frac{R - y_q}{R} = 0. \tag{40}$$

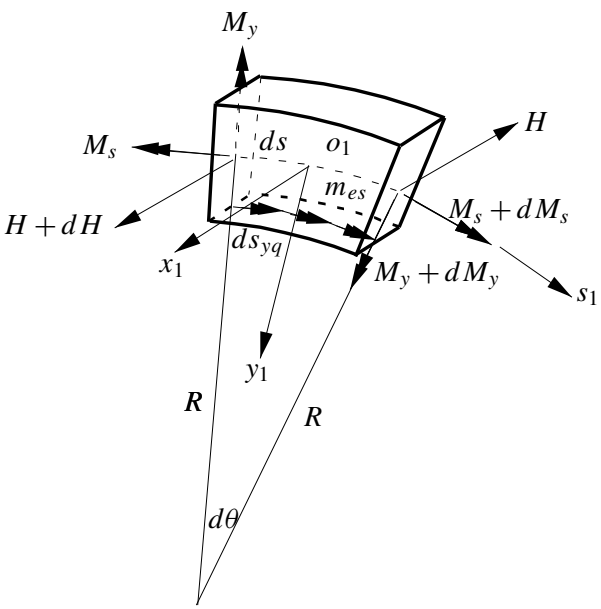

Figure 6. Lateral and torsional moment equilibrium.

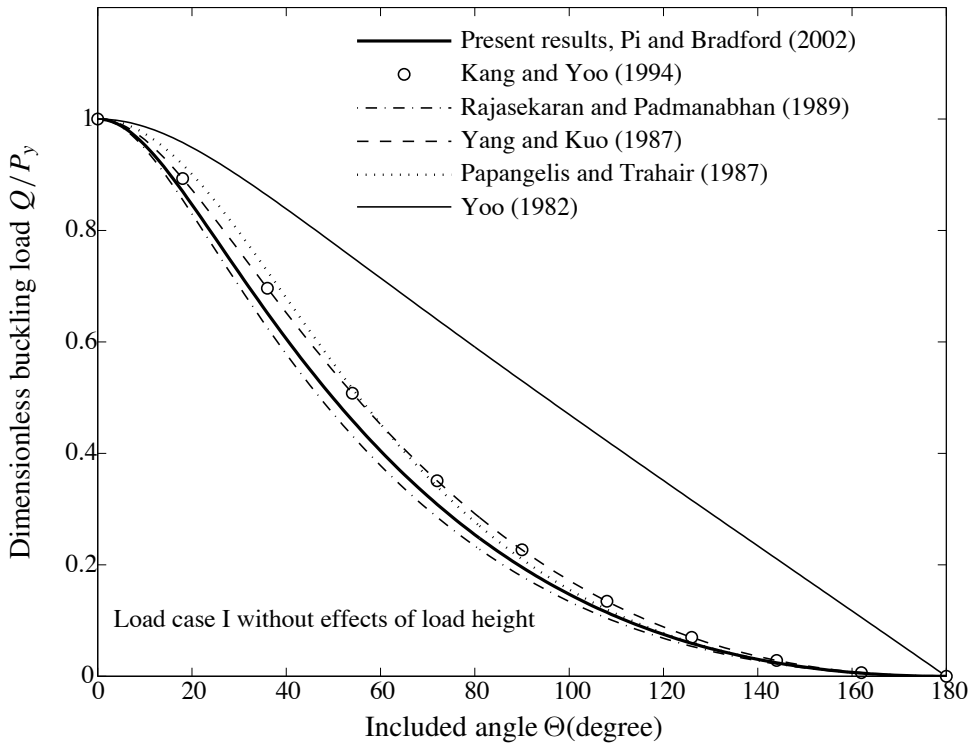

Figure 7. Comparison of buckling loads for load case I without effects of load height with the results of other researchers.

For torsional moment equilibrium, it can be shown from Figure 6 that

$$(M_s + \mathrm{d}M_s) - M_s - 2M_y \sin\frac{\mathrm{d}\theta}{2} + m_s \mathrm{d}s_{sq} = \mathrm{d}M_s - \frac{M_y}{R}\,\mathrm{d}s + m_{es}\frac{R - y_q}{R}\,\mathrm{d}s = 0,$$

which gives the differential equilibrium equation for the torsional buckling deformation

$$\frac{\mathrm{d}M_s}{\mathrm{d}s} - \frac{M_y}{R} + m_{es}\frac{R - y_q}{R} = 0. \tag{41}$$

Here the distributed torques m_{es} produced by the lateral and radial components q_{ex} and q_{ey} of the loads q at the load height y_q are given by

$$m_{es} = q_{ey} y_q \phi + q_{ex} y_q. \tag{42}$$

Substituting the expressions for Q_{ex}, M_s, M_y, and m_{es} given by Equations (34)–(35) and (42) into Equations (40) and (41) leads to the same differential equilibrium equations as those given by Equations (14) and (15).

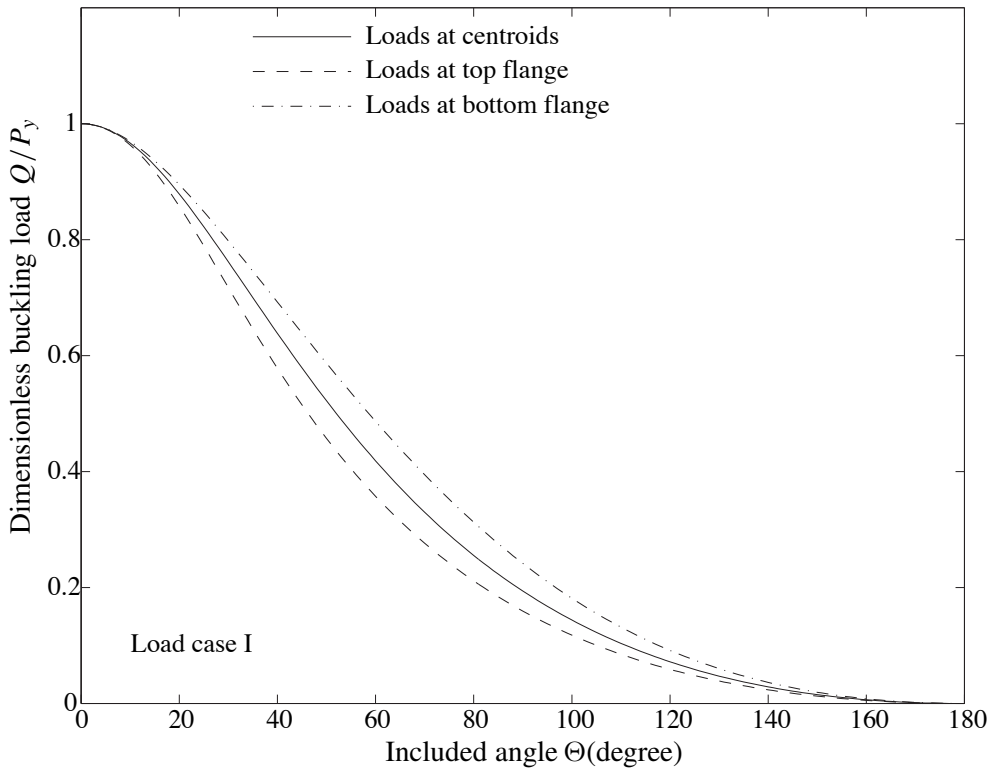

Figure 8. Effects of load height on buckling loads for load case I.

5. Numerical examples and comparisons

5.1. ***Comparison with solutions by other researchers for load case I.*** A number of researchers [Yoo 1982; Papangelis and Trahair 1987; Yang and Kuo 1987; Rajasekaran and Padmanabhan 1989; Kang and Yoo 1994; Bradford and Pi 2002] have obtained closed form solutions for the flexural-torsional buckling load for arches under uniform compression when the uniformly distributed radial dead loads act at the centroid (the load case I). In this case, the load height $y_q = 0$ and the solution for the buckling load given by Equations (30) and (31) become

$$\left(\frac{Q}{P_{yn}}\right)^2 - \left(\left(1+\frac{a_n^2}{b_n^2}\right)\frac{P_{sn}}{P_{yn}} + \left(1-a_n^2\right)^2\right)\frac{Q}{P_{yn}} + (1-a_n^2)^2\frac{P_{sn}}{P_{yn}} = 0, \tag{43}$$

the same results as those obtained by Bradford and Pi [2002].

Solutions for the first mode flexural-torsional buckling load of arches under uniform compression given by Equation (43) are compared with the solutions by other researchers in Figure 7 for arches with an Australian I-section 1200WB249 ($A = 31700$ mm^2, $I_x = 6380 \times 10^6$ mm^4, $I_y = 87 \times 10^6$ mm^4, $J = 4310 \times 10^3$ mm^4, $I_w = 28500 \times 10^9$ mm^6, $E = 200,000$ MPa, $\nu = 0.3$) [BHP 2000] and with the length $S = 5000$ mm. Because the length S is constant, the curvature $1/R$ increases with an increase of the included angle Θ. It can be seen that there are some differences between the results. In particular, the result of Yoo [1982] (based on the method of a forced analogy of curved members

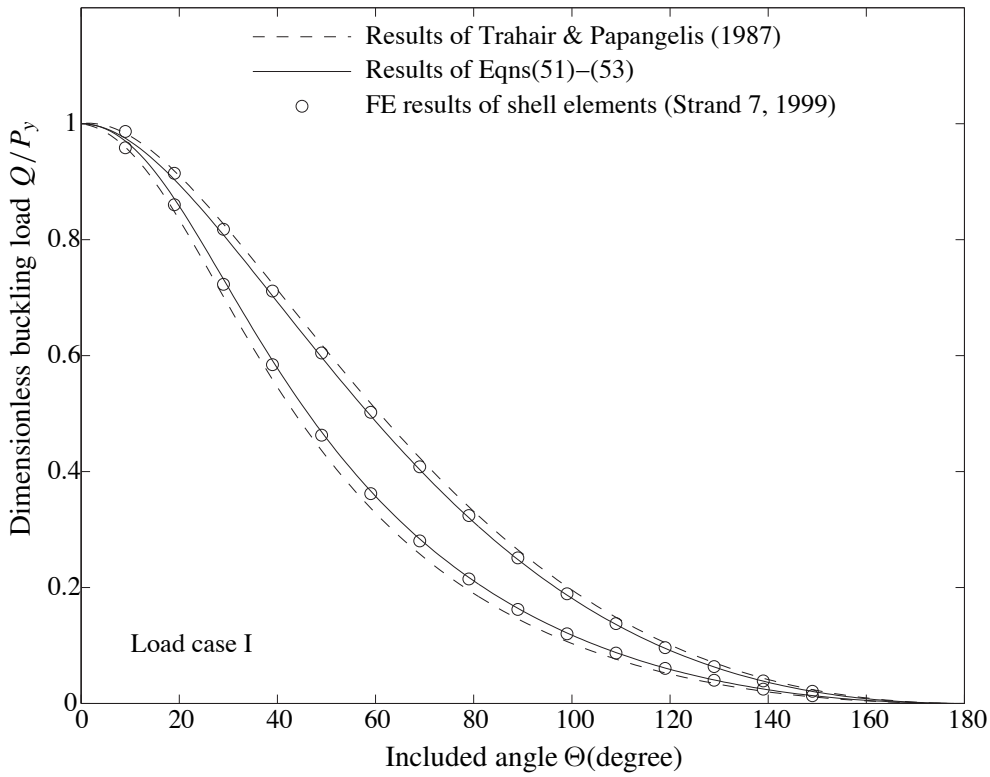

Figure 9. Comparison of effects of load height on buckling loads with results of FE and other results for load case I.

to straight members) diverges substantially from those of the others. It is worth pointing out that the solution methods used by most of these researchers [Papangelis and Trahair 1987; Yang and Kuo 1987; Rajasekaran and Padmanabhan 1989; Kang and Yoo 1994; Bradford and Pi 2002] are correct. The minor discrepancies between the results are due to the fact that some small differences in the terms of the strain-displacement relationship were obtained when different methods of derivation were used. Researchers such as [Papangelis and Trahair 1987; Yang and Kuo 1987; Rajasekaran and Padmanabhan 1989; Kang and Yoo 1994; Bradford and Pi 2002] have also presented comparisons and analyses of these discrepancies.

5.2. ***Effects of load height.*** Solutions for the first mode flexural-torsional buckling loads of arches subjected to radial dead loads (load case I) and acting at the top, the centroid, and the bottom of the cross-section are compared in Figure 8. These arches have an Australian steel I-section 250UB25 ($A = 3270$ mm^2, $I_x = 35.4 \times 10^6$ mm^4, $I_y = 2.55 \times 10^6$ mm^4, $J = 67.4 \times 10^3$ mm^4, $I_w = 36.7 \times 10^9$ mm^6 $E = 200,000$ MPa and Poisson's ratio $\nu = 0.3$) [BHP 2000] and the length $S = 2000$ mm. It can be seen that when the radial loads act at the centroid, the buckling load is lower than when the radial loads act at the bottom of the cross-section, but it is higher than when the radial loads act at the top of the cross-section. The difference between these buckling loads increases with an increase of the included angle of the arch, and then decreases with a further increase of the included angle of the arch.

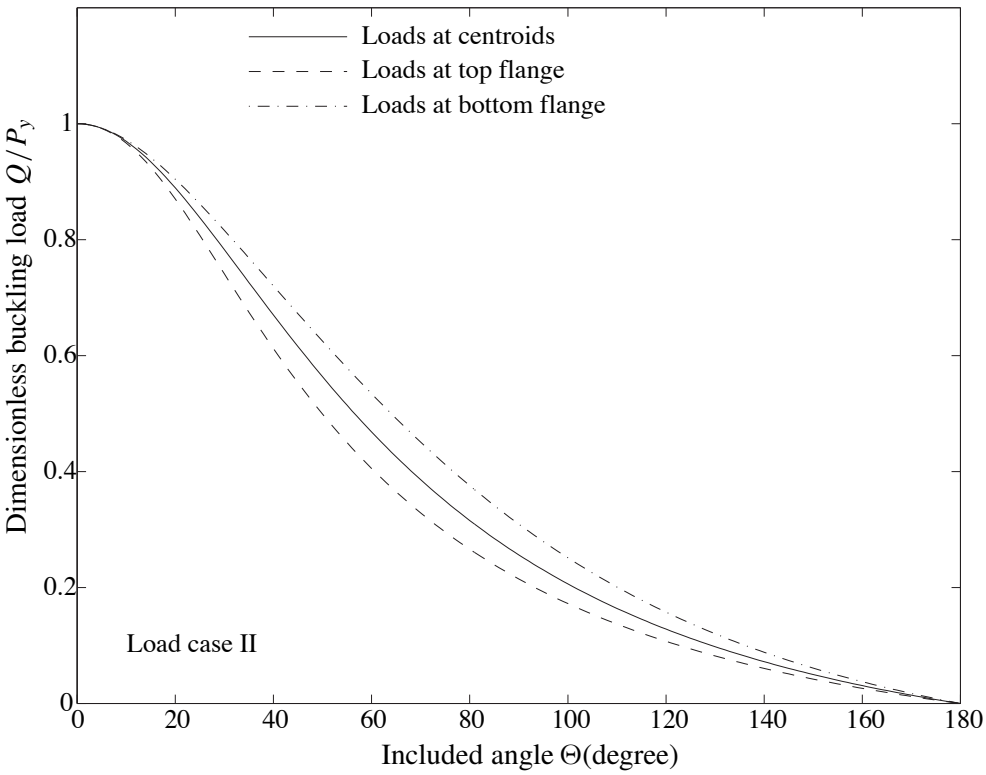

Figure 10. Effects of load height on buckling loads for load case II.

Trahair and Papangelis [1987] and Trahair [1993] studied the effects of load height on the flexural-torsional buckling of arches under uniform compression for case I. Trahair [1993] used diagrams to show the effects without giving analytical solutions, while Trahair and Papangelis [1987] obtained an analytical solution. The solutions of Equations (30)–(31) for load case I are compared with their solutions in Figure 9. Also shown in Figure 9 are results which were are obtained by an eigenvalue analysis using the 8-noded shell elements of the FE package [Strand7 1999] to verify the solutions Equations (30)–(31). The FE results agree with the solutions of Equations (30)–(31) very well. Trahair and Papangelis [1987] ignored the small term r_y^2/R^2, and their results are slightly lower than the FE results, while for bottom flange loading, their results are slightly higher than the FE results. However, the differences between them are very small and so the solutions of [Trahair and Papangelis 1987] are also accurate.

Figure 10 compares solutions for the first mode flexural-torsional buckling loads of arches subjected to radial loads that are always directed towards the arch center during buckling (the load case II) and are acting at the top, at the centroid, and at the bottom of the cross-section for arches with an I-section 250UB25 and length $S = 2000$ mm. It can be seen that when the radial loads act at the centroid, the buckling load is lower than that when they act at the bottom of the cross-section, but it is higher than when the radial loads act at the top of the cross-section. The difference between these buckling loads increases with an increase of the included angle of the arch, and then decreases with a further increase of the included angle of the arch.

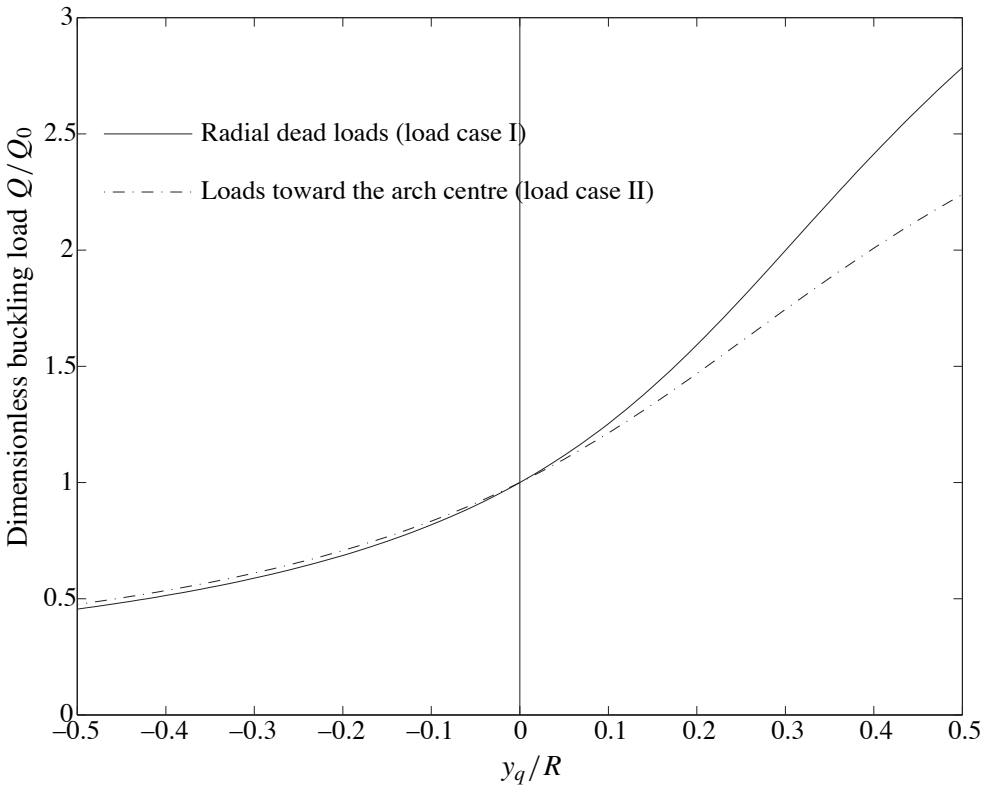

Figure 11. Comparison of effects of load height on buckling loads for load cases I and II.

Figure 11 compares the effects of the load height on the buckling loads of arches subjected to radial loads always directed to the arch center (load case II), given by Equations (30) and (32), with those for arches subjected to radial dead loads (load case I), given by Equations (30) and (31); in the figure, Q_0 is the buckling load when the loads act at the centroid. It can be seen that the effects of load height on the buckling loads only differ in a visible way when the loads act below the centroid (that is, y_q is positive as shown in Figures 1 and 4). In this case, the arches subjected to uniformly distributed radial dead loads experience higher buckling load increases, particularly for larger y_q values.

5.3. ***Comparison with Vlasov's solution for load case III.*** Solutions for the first mode of flexural-torsional buckling load of arches with an I-section 250UB25 and length $S = 2000$ mm under hydrostatic loads given by Equations (30) and (33) are compared in Figure 12 with the solution of [Vlasov 1961].

It can be seen from Figure 12 that the solution of [Vlasov 1961] is slightly lower than the present results, because he did not consider the coupling term contributed by the torsional moment M_{es} to the differential equilibrium equation for lateral deformations.

5.4. ***Arches with a narrow rectangular cross-section.*** Timoshenko and Gere [1961] investigated the flexural-torsional buckling of an arch with a narrow rectangular cross-section for the load cases I and II, but without considering the Wagner effects and warping. In this case, the virtual work

$$\left(-Qr_0^2(\phi' - u'/R)(\delta\phi' - \delta u'/R)\right),$$

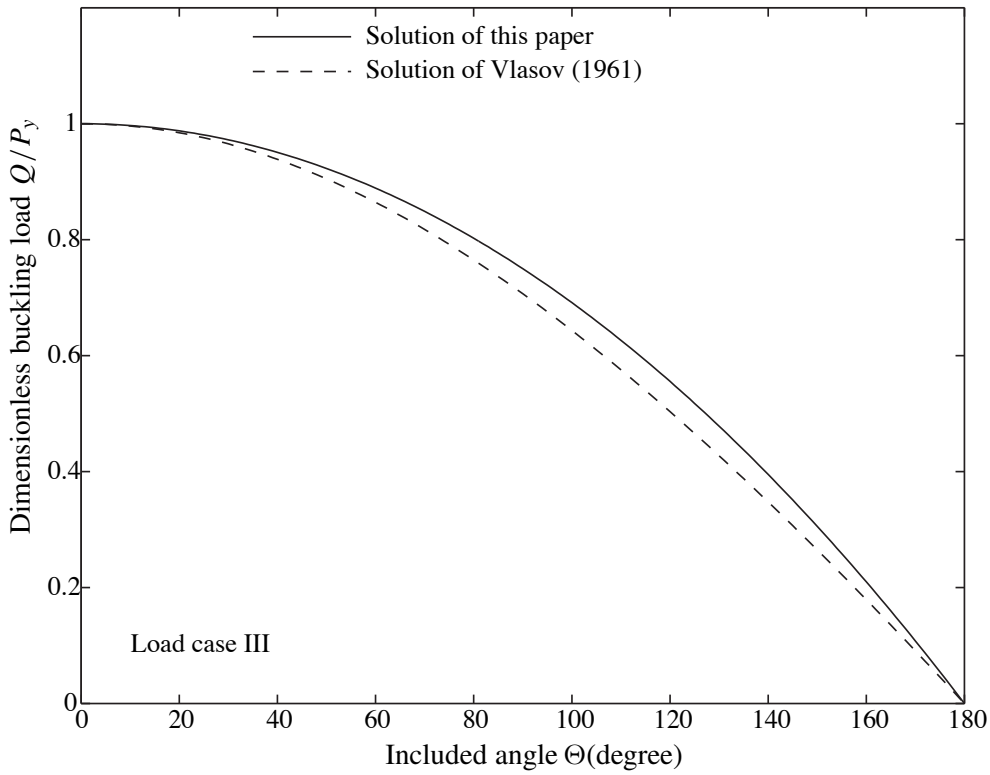

Figure 12. Comparison with Vlasov's solution for load case III.

due to Wagner effects, and

$$EI_w\left(\phi'' - u''/R\right)\left(\delta\phi'' - \delta u''/R\right),$$

due to warping in the virtual work statement given by Equation (13), are equal to zero, and accordingly the Wagner terms and warping torsion moments (Vlasov terms) in the differential equilibrium equations (14) and (15) vanish. The flexural-torsional buckling load for an arch with a narrow rectangular section can then be obtained from Equations (14) and (15), by considering the components of q_{ex} and q_{ey} of the load q being given by Equations (21)–(23) respectively, as

$$\frac{Q}{P_{yn}} = \begin{cases} \frac{(1-a_n^2)^2}{1+a_n^2/b_n^2}, & \text{for the case of radial dead loads,} \\ \frac{1-a_n^2}{1+a_n^2/b_n^2}, & \text{for the case of directed radial loads,} \\ 1-a_n^2, & \text{for the case of hydrostatic loads.} \end{cases} \tag{44}$$

The solutions given by Equation (44) are the same as those of [Timoshenko and Gere 1961].

6. Conclusions

This paper has used both virtual work and equilibrium approaches to investigate the elastic flexural-torsional buckling of circular arches under uniform compression produced by uniformly distributed radial

dead loads, by hydrostatic loads or by uniformly distributed directed radial loads. The effects of the load height on the buckling loads have also been studied, and solutions for the buckling loads for these loading cases, including the effects of the load height, have been obtained in closed form. It was found that the buckling load under hydrostatic loading is highest while the buckling load under uniform radial dead loading is the lowest. The lateral components of the uniformly distributed radial loads that are always directed toward the center of the initial curvature of the arch and those of the hydrostatic loads, too, increase the flexural-torsional buckling resistance of an arch under uniform compression. The buckling load increases as the load height below the centroid of the cross-section increases, while the buckling load decreases as the load height above the centroid of the cross-section increases.

References

[BHP 2000] BHP, *Hot rolled and structural steel products*, BHP, Melbourne, 2000.

[Bolotin 1963] V. V. Bolotin, *Nonconservative problems of theory of elastic stability*, Pergamon, Oxford, 1963.

[Bradford and Pi 2002] M. A. Bradford and Y. L. Pi, "Elastic flexural-torsional buckling of discretely restrained arches", *J. Struct. Eng.* (*ASCE*) **128**:6 (2002), 719–729.

[Burn 1985] R. P. Burn, *Groups: A path to geometry*, Cambridge University Press, Cambridge, 1985.

[Guran 2000] A. Guran, *Theory of elasticity for scientists and engineers*, Birkhauser, Boston, MA, 2000.

[Hodges 2006] D. H. Hodges, *Nonlinear composite beam theory*, AIAA, Reston, VA, 2006.

[Ings and Trahair 1987] N. L. Ings and N. S. Trahair, "Beam and column buckling under directed loading", *J. Struct. Eng.* (*ASCE*) **113**:6 (1987), 1251–1263.

[Kang and Yoo 1994] Y. J. Kang and C. H. Yoo, "Thin-walled curved beams, II: Analytical solutions for buckling of arches", *J. Eng. Mech.* (*ASCE*) **120**:10 (1994), 2102–2125.

[Papangelis and Trahair 1987] J. P. Papangelis and N. S. Trahair, "Flexural-torsional buckling of arches", *J. Struct. Eng.* (*ASCE*) **113**:4 (1987), 889–906.

[Pi and Bradford 2004] Y. L. Pi and M. A. Bradford, "Effects of prebuckling deformations on the elastic flexural-torsional buckling of laterally fixed arches", *Int. J. Mech. Sci.* **46**:2 (2004), 321–342.

[Rajasekaran and Padmanabhan 1989] S. Rajasekaran and S. Padmanabhan, "Equations of curved beams", *J. Eng. Mech.* (*ASCE*) **115**:5 (1989), 1094–1111.

[Simitses 1976] G. J. Simitses, *An introduction to the elastic stability of structures*, Prentice-Hall, Englewood Cliffs, NJ, 1976.

[Simitses and Hodges 2006] G. J. Simitses and D. H. Hodges, *Fundamentals of structural stability of structures*, Elsevier, Boston, MA, 2006.

[Strand7 1999] *Using Strand7: Introduction to the Strand 7 finite element analysis system*, G+D Computing, Sydney, 1999, Available at http://www.strand7.com/Downloads/Using%20Strand7%20Manual.zip.

[Timoshenko and Gere 1961] S. P. Timoshenko and J. M. Gere, *Theory of elastic stability*, 2nd ed., McGraw-Hill, New York, 1961.

[Trahair 1993] N. S. Trahair, *Flexural-torsional buckling of structures*, E&FN Spon, London, 1993.

[Trahair and Bradford 1998] N. S. Trahair and M. A. Bradford, *The behaviour and design of steel structures to AS4100*, E&FN Spon, London, 1998.

[Trahair and Papangelis 1987] N. S. Trahair and J. P. Papangelis, "Flexural-torsional buckling of monosymmetric arches", *J. Struct. Eng.* (*ASCE*) **113**:10 (1987), 2271–2288.

[Vlasov 1961] V. Z. Vlasov, *Thin-walled elastic beams*, 2nd ed., Israel Program for Scientific Translation, Jerusalem, 1961.

[Yang and Kuo 1987] Y. B. Yang and S. R. Kuo, "Effects of curvature on stability of curved beams", *J. Struct. Eng.* (*ASCE*) **113**:6 (1987), 821–841.

[Yoo 1982] C. H. Yoo, "Flexural-torsional stability of curved beams", *J. Eng. Mech. Div.* (*ASCE*) **108**:6 (1982), 1351–1369.

Received 11 Dec 2005. Revised 22 Mar 2006. Accepted 3 Apr 2006.

MARK ANDREW BRADFORD: m.bradford@unsw.edu.au
School of Civil and Environmental Engineering, The University of New South Wales, Sydney, NSW 2052, Australia

YONG-LIN PI: y.pi@unsw.edu.au
School of Civil and Environmental Engineering, The University of New South Wales, Sydney, NSW 2052, Australia